ENERGY AND EXERGY ANALYSIS OF AN AIR-COOLED GEOTHERMAL POWER PLANT WITH FIXED NOZZLE TURBINE IN SUBSONIC EXPANSION AND SUPERSONIC EXPANSION VIA CFD ANALYSIS

Choon Seng Wong[1] and Susan Krumdieck[2]

[1,2]Department of Mechanical Engineering, University of Canterbury, Private Bag 4800, Christchurch, 8041, New Zealand

[1]choon.wong@pg.canterbury.ac.nz

[2]susan.krumdieck@canterbury.ac.nz

Keywords: *Air-cooled geothermal plant, Organic Rankine Cycle, Supersonic Expansion, Fixed geometry turbine, CFD Analysis.*

ABSTRACT

The performance of air-cooled geothermal power plants is susceptible to the changes in ambient temperature especially in New Zealand due to the large difference in the atmospheric temperature for summer and winter seasons. The turbine is typically designed for a specific set of operating conditions, but the operating conditions also change with the resource enthalpy and the heat sink temperature. The effect of the fluctuation in the condenser temperature due to the changes in ambient temperature affects the pressure ratio across the turbine, thus reducing the efficiency of the turbine. This paper investigates the potential for adapting a 100 kW gas turbine with fixed nozzle vanes into an ORC turbine. An air-cooled ORC system was designed using the geothermal source conditions and the mean daily temperature in Rotokawa, New Zealand. The effect of the air temperature on the condenser temperature, and thus on the operation of the turbine was studied. The performance of the turbine was studied via computational fluid dynamic (CFD) tools with different pressure ratio to take into account of subsonic expansion and supersonic expansion across the selected turbine in a single stage configuration. The turbine performance curve was then incorporated into the ORC system and the efficiency map of the ORC system using the common fluids, namely isobutane, R245fa and R134a, was generated. The model results were used to develop a correlation between the ambient temperature and the performance of the ORC system.

1. INTRODUCTION

The demand for Geothermal Energy is increasing continuously. Twenty four countries generated electricity from geothermal resources with total installed capacity of 8,930 MWe in year 2005 (Bertani, 2005). The total installed capacity increased up to 10,898 MWe in year 2010 (Bertani, 2012). Geothermal plant can be classified into a number of different categories: single flash, double flash, binary plant, hybrid or combined cycle (DiPippo, 2012). The type of the geothermal plant is dependent on the quality of the brine, temperature of the heat source and the condition of the geothermal reservoir. Single flash plant is by far the most popular geothermal plant with the highest installed capacity of 41% of the total capacity of the geothermal plant based on the data taken from WGC2010 (Bertani, 2012). Binary plant has the least installed capacity at 11% but the number of units is twice the number of units of single flash plant and quadruple of units of double flash plants (Bertani, 2012).

Binary plant can be cooled via water-cooling and/or air-cooling. Chena Geothermal ORC plant is water-cooled during summer and air-cooled during winter to maximize the cycle performance (Holdmann, 2007). Of course, water-cooling is favored over air-cooling due to the much higher heat capacity and heat transfer coefficient of water compared to dry air (Mendrinos, Kontoleontos, & Karytsas, 2012). Dry cooling induces an extra installation cost and operational cost, up to ten times more than the water cooling system in a similar size to the air cooling system (Li, Pei, Li, Wang, & Ji, 2012). The air-cooling is still commonly used in New Zealand geothermal plants in Rotokawa (Legmann & Sullivan, 2003), Wairakei (Thain & Carey, 2009), Mokai, and Ngawha (Dunstall, 1999) due to the geographical location and lack of access to a water body.

Seasonal ambient temperature variation has been shown to reduce the plant net power output by up to 40% from winter to summer in northern Nevada (Kanoğlu & Çengel, 1999). The exergy efficiency reduces with increasing ambient temperature, indicating the degradation in plant performance (Mines, 2002). Operation of geothermal plant away from the design point ambient temperature changes performance of the evaporator, pump and condenser (Wendt & Mines, 2011).

Several researchers have investigated the off-design effects of the ORC on the turbine. The change in ambient temperature contributes to off-design performance of the turbo-generator. Greg (Mines, 2002) has modelled the turbine off-design performance as a deviation from the velocity ratio using the corrections chart from Balje (Balje, 1981). The turbine correlation chart developed by Balje, however, is limited to incompressible fluids (Balje, 1981). The turbine-generator efficiency was assumed to be constant by Cengel (Kanoğlu & Çengel, 1999) and Marco (Astolfi, Romano, Bombarda, & Macchi, 2014) in modelling the binary geothermal plant. Mitsos modeled the turbine performance with isobutane as a function of the design isentropic efficiency, ratio of enthalpy drop and ratio of volumetric flow rate (Ghasemi, Paci, Tizzanini, & Mitsos, 2013).

This study aims to investigate the performance of the turbine with different working fluids at different pressure ratio using CFD modeling. An existing 100 kW gas turbine with published geometry data (Sauret, 2012) was adapted for the ORC unit in this study. The performance of the turbine using different fluids was conducted using ANSYS-CFX. A binary plant model was developed in Engineering Equation Solver (EES). The analysis was performed using the actual heat source conditions from the Rotokawa binary plant (Legmann & Sullivan, 2003) and the ambient temperature profile in Taupo in the year 2012 (NIWA, 2014) to determine the pressure ratio across the turbine. Four different working fluids are studied, namely n-Pentane, isobutane, R245fa, and R134a. The fluids are chosen as they are commonly used in

commercial ORC units; R134a in Chena binary plant (Aneke, Agnew, & Underwood, 2011), isobutane in Otake pilot plant in Japan (DiPippo, 2004) and the plant operated by ENEL (Ghasemi et al., 2013), and n-Pentane in ORMAT Energy Convertor in Brady (DiPippo, 2004), and Rotokawa (Legmann & Sullivan, 2003). R245fa was reported as the most suitable candidate in geothermal application with geothermal brine temperature over 167°C when thermodynamic First-Law efficiency is the objective function (Holdmann, 2007). The performance curve of the turbine with different fluids is then incorporated into the cycle model to investigate the net power output, thermal efficiency (also known as thermodynamic First-Law efficiency), and exergy efficiency (known as Second-Law efficiency) of the cycle and the turbine as a function of ambient temperature.

2. METHODOLOGY

Given the heat source condition in Rotokawa and the ambient temperature near Rotokawa, a binary cycle model using an air-cooled condenser was developed using a market available gas turbine. The turbine performance was evaluated via CFD tools to predict the performance behavior using different fluids. The performance curve was then incorporated into the binary cycle for energy analysis and exergy analysis on the turbine and the binary cycle. The overall analysis strategy is shown in Fig. 1.

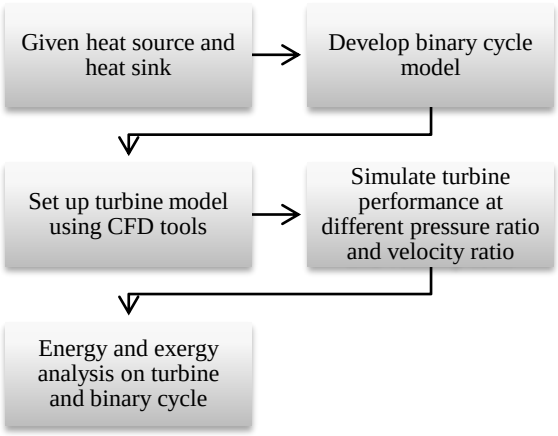

Figure 1: Flow Chart of Analysis Strategy

2.1 Binary Cycle Model with Air-Cooled Condenser

The basic binary cycle model without recuperator was developed as shown in Fig. 2 (zero mass flow rate into the recuperator). The brine condition into the binary plant in Rotokawa (Legmann & Sullivan, 2003), has the following thermodynamic operating conditions.

- Brine inlet temperature: 217.5°C
- Brine outlet temperature: 150°C
- Design ambient temperature: 12°C

The following assumptions were made during the simulation:

- Negligible pressure loss across the heat exchangers and pipe fittings
- Ideal heat transfer across the heat exchangers
- Pressure loss across the piping is negligible
- Air side pressure drop in the air cooled-condenser is 170 Pa (Lukawski, 2010)
- Degree of sub-cooling: 0°C
- Differential temperature at the condenser pinch: 5°C
- Fan efficiency: 80%
- Generator efficiency: 95%
- Pump efficiency: 80%

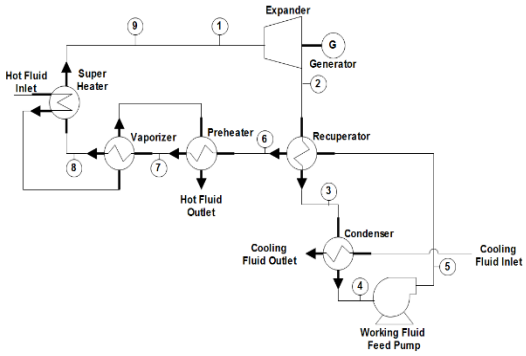

Figure 2: Basic geothermal binary plant

The basic energy balance cycle analysis was used as described in the text by DiPippo (DiPippo, 2012). The power output from the turbine was determined as a function of the change in total enthalpy across the turbine, total-to-total efficiency and the mass flow of the fluid.

$$W_{turbine} = m\eta_{gen}\eta_{tt}\Delta h_{tt,is} = m\eta_{gen}\eta_{ts}\Delta h_{ts,is} \qquad (1)$$

$W_{turbine}$ is the power output of the turbine, η_{gen} is the electrical conversion efficiency of generator, η_{ts} is the total-to-static efficiency of the turbine, η_{tt} is the total-to-total efficiency of the turbine, $\Delta h_{tt,is}$ and $\Delta h_{ts,is}$ are the change of enthalpy of the working fluid across the turbine during an isentropic expansion process, evaluated at total-to-total condition and total-to-static condition respectively.

The fan power of the air-cooled condenser, W_{fan}, was determined as a function of total air side pressure loss, Δp_{air}, the velocity of the air flow, V_{air} and efficiency of the fan, η_{fan}.

$$W_{fan} = \frac{V_{air}\left(\Delta p_{air}\right)}{\eta_{fan}} \qquad (2)$$

The air side pressure drop was assumed constant at 170 Pa (Lukawski, 2010). The new power output, W_{net}, is equal to the power produced from the turbo-generator, $W_{turbine,}$ minus the parasitic loss of the pump power, W_{pump} and the auxiliary power from the air-cooled condenser, W_{fan}.

$$W_{net} = W_{turbine} - W_{fan} - W_{pump} \qquad (3)$$

The ambient temperature profile in Taupo (11 km from Rotokawa) was selected to model the binary plant behavior, where the latitude is -38.68°, the longitude is 176.07°, and the height is 385m based on the NIWA climate database (NIWA, 2014). The temperature data in year 2012 was extracted, with mean monthly air temperature, mean daily maximum, and mean daily minimum air temperature, as shown in Fig. 3.

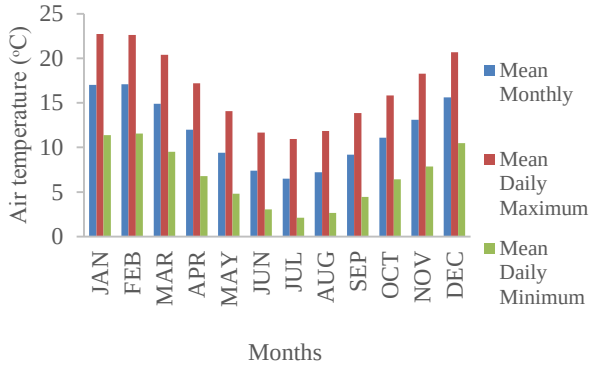

Figure 3: Average air temperature in Taupo in year 2012

2.2 Turbine Analysis using CFD Tools

An existing gas turbine with published geometry data (Sauret, 2012) was adapted as an ORC turbine in this study. The gas turbine was initially designed for air at high speed operation, at 106,588 rev/min with nominal power of 100 kW. The turbine model was regenerated using ANSYS Turbomachinery Package and validated against the experimental data. The CAD model of the turbine stage (nozzle and impeller) was generated using ANSYS BladeGen (in Fig. 4) and the meshing was performed using ANSYS TurboGrid.

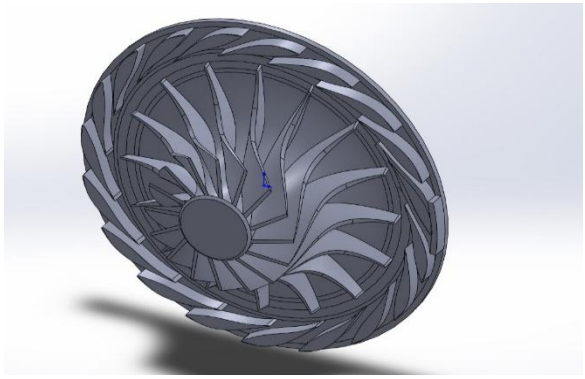

Figure 4: CAD model of nozzle and impeller

Steady state analysis was performed via ANSYS-CFX 14.5 to determine the overall performance of the turbine stage. *Frozen rotor* was set in ANSYS-CFX to take account of the non-axisymmetric flow between the nozzle and the impeller. The model was first validated using air with the published experimental data (Jones, 1996). The trend of the turbine performance was re-generated with a shift to the lower velocity ratio (as shown in Fig 5). The peak efficiency was predicted at a velocity ratio of 0.6, instead of the actual value of 0.74. The shift might be attributed to the lack of details in the geometry of the trailing edge of the turbine wheel. The pressure recovery factor of the diffuser from the CFD model deviates slightly from the experimental data, and this further contributes to the model error. A correction factor was used to achieve the CFD model with the experimental velocity ratio. The corrected CFD model agrees with the experimental data with error less than 1% in the efficiency. The subsequent analysis was then conducted with the corrected CFD model assuming the absence of the diffuser.

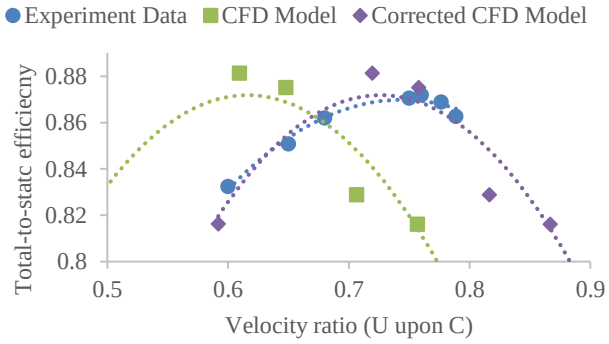

Figure 5: Comparison of the CFD model and the experimental data at different rotational speed

2.3 Thermodynamics First Law and Second Law Analysis

2.3.1 Turbine Parameters

The operation of the gas turbine using other working fluids, refrigerant and hydrocarbon with heavy molecular weight, requires a lower rotational speed, where the rotational speed can be determined at the optimal velocity ratio.

$$\frac{U}{C} = \frac{U}{\sqrt{2\Delta h_{is}}} \tag{4}$$

U is the tip speed of the impeller, C is the velocity of the fluid if the fluid is expanded in an ideal nozzle with the equivalent pressure ratio, and Δh_{is} is the change of enthalpy across the turbine in an isentropic process at a given pressure ratio. The thermal efficiency, $\eta_{I,turbine}$ (thermodynamic First-Law efficiency) and the functional exergy efficiency, $\eta_{II,turbine}$ (thermodynamic Second-Law efficiency) of the turbine are discussed below, and the details can also be found from the work by DiPippo (DiPippo, 2012).

$$\eta_{I,turbine} = \frac{h_{01} - h_{02}}{h_{01} - h_{2,is}} \tag{5}$$

h_{01} and h_{02} represent total enthalpy (stagnation enthalpy) at the turbine inlet and the turbine outlet, and $h_{2,is}$ is the isentropic enthalpy at the turbine outlet.

$$\eta_{II,turbine} = \frac{h_{01} - h_{02}}{(h_{01} - h_{02}) + T_0(s_2 - s_1)} \tag{6}$$

T_0 is the dead state temperature, where the dead state temperature of the air-cooled binary plant is the ambient temperature (or dry bulb temperature of the air), and s is the entropy at the assigned station.

2.3.2 Cycle Performance

The maximum theoretical thermal efficiency of a thermodynamic cycle is typically represented by Carnot efficiency with an isothermal heat addition at the heat source temperature and an isothermal heat rejection at the heat sink temperature. The brine, however, does not serve as an isothermal heat source since the brine temperature decreases during the heat transfer process. DiPippo has proposed a

triangular cycle efficiency with an isobaric heat addition process to better represent the possible maximum cycle efficiency (DiPippo, 2012). The triangular cycle efficiency, η_{TRI} can be found given the heat source and heat sink temperature.

$$\eta_{TRI} = \frac{T_H - T_L}{T_H + T_L} \quad (7)$$

T_H is the heat source temperature, the brine inlet temperature, and T_L is the heat sink temperature, the ambient air temperature. The thermal efficiency of the binary plant, $\eta_{I,cycle}$ is defined as the ratio of the net power output, W_{net} to the thermal energy input, Q_{in}.

$$\eta_{I,cycle} = \frac{W_{net}}{Q_{in}} \quad (8)$$

Q_{in} is the total heat addition into the working fluid in the preheater, vaporizer, and superheater. The exergy efficiency of the cycle, $\eta_{II,cycle}$, also known as utilization efficiency by DiPippo (DiPippo, 2012), is defined as the ratio of the net plant power output to the maximum theoretical power from the geothermal brine, considering the surrounding temperature.

$$\eta_{II,cycle} = \frac{W_{net}}{m_{gb}\left[\left(h_{gb,in} - h_0\right) - T_0\left(s_{gb,in} - s_0\right)\right]} \quad (9)$$

m_{gb} is the mass flow rate of the geothermal brine, $h_{gb,in}$ and h_0 are enthalpy of the geothermal brine evaluated at the inlet into the pre-heater and the dead state temperature respectively, and $s_{gb,in}$ and s_0 are entropy of the geothermal brine evaluated at the inlet into the pre-heater and the dead state temperature respectively. In general, binary plants have lower thermal efficiency than steam plants and geothermal flash plants as the temperature difference between the heat source and the heat sink temperature is smaller (Zarrouk & Moon, 2014).

3. RESULTS

3.1 Determination of Turbine Operating Conditions via Cycle Simulation

Refrigerants can be classified into wet, dry and isentropic fluids depending on the slope of the saturation curve. R134a is classified as wet fluid, R245fa as isentropic fluid, and n-Pentane and isobutane (R600a) as dry fluid (Chen, Goswami, & Stefanakos, 2010). A large amount of superheat is required for wet fluid to avoid the formation of liquid droplet at the turbine outlet and prevent the damage of the turbine wheel from cavitation effects.

R134a is superheated up to 10°C to avoid wet expansion. Superheat for dry fluid and isentropic fluid would reduce the overall cycle efficiency, as a larger amount of heat at the turbine outlet has to be rejected to the atmosphere (Chen et al., 2010). This would require a larger heat transfer area or a more powerful fan for the condenser, which incurs higher installation or operational cost.

The installation cost and the operational cost of a plant is also a function of the maximum allowable pressure. The maximum allowable pressure was limited below 2,500 kPa to avoid the application of high-pressurized piping and equipment. The cycle simulation was performed under sub-critical condition to avoid the cycle from operating in trans-critical pressure condition. The turbine inlet condition and the pressure ratio across the selected gas turbine were obtained from the cycle simulation assuming a constant turbine efficiency at 80%.

Table 1: Turbine inlet condition

Fluid	*R134a*	*n-Pentane*	*Isobutane*	*R245fa*
Type	Wet	dry	Dry	isentropic
T_{in} *(C)*	85	178	113	133
P_{in} *(kPa)*	2,366	2,427	2,381	2,339
Pressure ratio	2.4	25	4.7	10.2
Degree of superheat (C)	10	3	3	3
η_{cycle}	5.9 %	15.4%	10.0 %	12.1%
Nominal Power (kW)	55 kW	300 kW	80 kW	135 kW

There is a significant difference in possible plant performance for the same configuration, the same turbine efficiency, and the same temperatures due solely to the working fluid thermodynamic behavior. The maximum cycle efficiency was achieved by n-Pentane, in line with the maximum cycle temperature, according to the Eq. (7). Note that the pressure ratio for n-Pentane is too high for a radial turbine and would require a multiple-stage axial turbine.

3.2 Evaluation of Turbine Expansion Process via CFD Model

The turbine performance was simulated using CFD tools for the given operating condition from Table 1.

3.2.1 Turbine Behavior at Different Pressure Ratio and Velocity Ratio

Turbine performance was modeled for each working fluid, except n-Pentane, at different velocity ratio to determine the optimal rotational speed of the turbine, as shown in Fig. 5. The optimal velocity ratio was determined to be in the range of 0.6 and 0.7 from Fig. 6, which corresponds to the experimental data of by Jones (Jones, 1996) and the study by Baines (Moustapha, Zelesky, Baines, & Japiske, 2003). The design speed of the turbine, the gear ratio to couple the turbine to a 60Hz generator, and the optimal velocity ratio were tabulated in Table 2.

Table 2: Optimal rotational speed of single stage gas turbine with different working fluids

Fluids	*Pressure Ratio*	*Gear ratio*	*Rotational Speed (rev/min)*	*U/C*
R245fa	10.2	8	28,800	0.607
Iso-butane	4.7	11	39,600	0.675
R134a	2.4	6	21,600	0.710

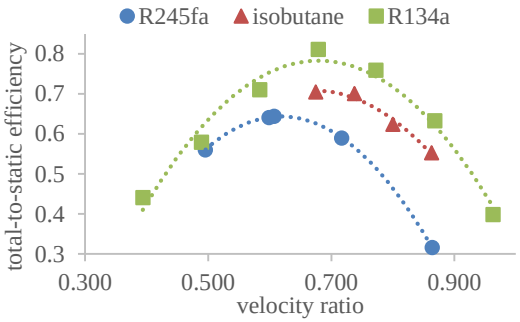

Figure 6: Performance analysis of gas turbine using refrigerants at different velocity ratio

The turbine performance was then simulated at different pressure ratios at the given velocity ratio in Table 2. R134a shows a higher total-to-static efficiency, followed by R245fa and isobutane. A low pressure ratio is preferable for single-stage radial turbines for optimal performance for all three fluids, as shown in Fig. 7.

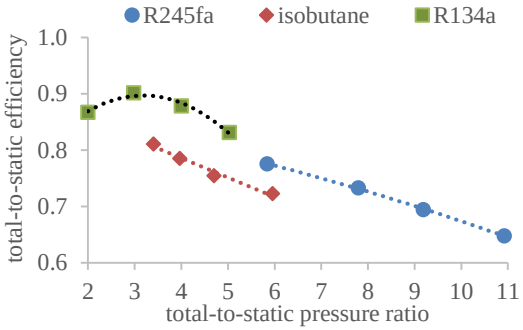

Figure 7: Performance analysis of gas turbine as a function of pressure ratio using different working fluids at optimal velocity ratio

3.2.2 Sub-sonic Expansion vs. Super-sonic Expansion

A complete solution of the flow field was generated for the gas turbine using different fluids, R134a, isobutane and R245fa. R134a and isobutane operating in subsonic expansion show a higher turbine efficiency than R245fa in supersonic expansion process, as shown in Fig. 6. The discrepancy in the efficiency is attributed to the design of the turbine blade passage. The gas turbine was originally designed for subsonic expansion using air as the working fluid (Jones, 1996). A minimum cross-sectional area, known as the throat, exists near the trailing edge of the blade passage. The throat area determines the flow capacity across the blade passage and allows proper diffusion of flow at the trailing edge of the blade. Diffusion is required to control the swirl angle of the flow near the turbine outlet and recover the kinetic energy of the flow, which in turn controls the specific work output, W_x from the turbine, based on Euler turbomachinery relation, as shown in eq.(10).

$$W_x = U_1 C_{m,1} \tan\alpha_1 - U_2 C_{m,2} \tan\alpha_2 \qquad (10)$$

Where U is the tip speed of the turbine, C_m is the absolute meridional flow velocity, and α is the absolute flow angle, at the assigned station. Station 1 represents the turbine inlet and station 2 represents the turbine outlet. The velocity vector of R134a in Fig. 8 shows a smooth flow pattern along the blade passage with minimal secondary flow losses. The low flow velocity at the turbine outlet increases the specific work output of the turbine, as shown in Eq. (10).

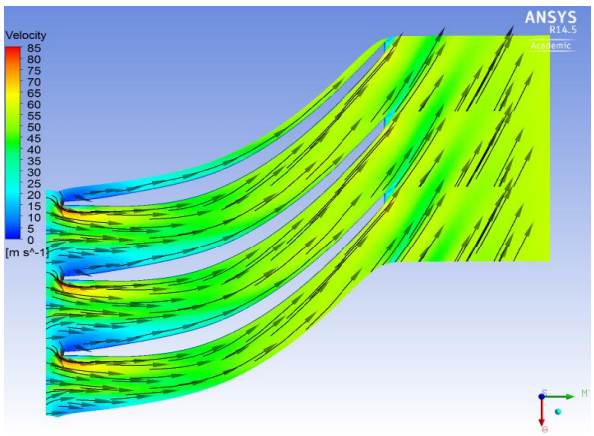

Figure 8: Velocity vector of R134a along the blade passage

The high pressure ratio across the turbine using R245fa produces a supersonic expansion process in the turbine. The flow accelerates up to the throat along the blade passage, similar to the subsonic expansion. The flow continues to accelerate downstream of the throat and the absolute flow velocity increases significantly up to 280 m/s, as shown in Fig. 9. The over-acceleration of the flow at the downstream of the throat reduces the specific work output of the turbine stage, based on Eq. (10). The mismatch between the blade profile and the characteristics of supersonic expansion reduces the turbine stage efficiency and contributes to the discrepancy of the turbine efficiency between R134a, isobutane and R245fa in Fig. 6.

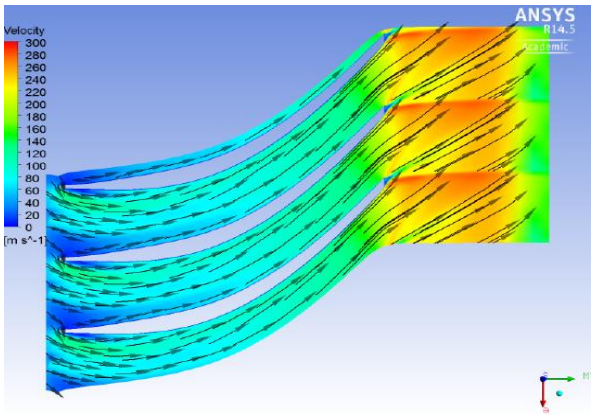

Figure 9: Velocity vector of R245fa along the blade passage

3.3 Energy Analysis and Exergy Analysis

Energy analysis was conducted on both the turbine and the binary cycle to determine the variation of thermal efficiency as a function of ambient temperature across the year. The maximum cycle efficiency was determined as triangular cycle efficiency, as discussed in Section 2.3.2. The triangular cycle efficiency across the year is plotted in Fig. 10. The thermal efficiency and the exergy efficiency of the turbine across the year using different fluids are given in Fig. 11. The thermal

efficiency and the exergy efficiency of the binary cycle are plotted as a function of ambient temperature in Fig. 13 and Fig. 14 respectively.

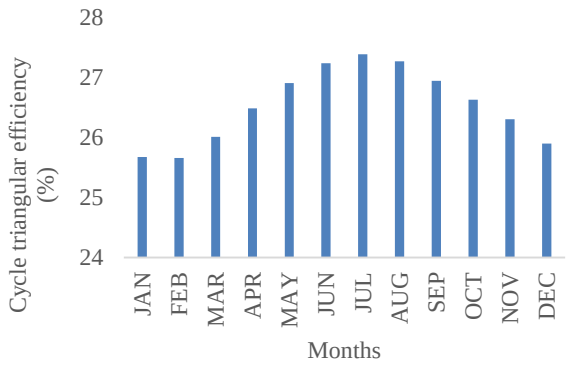

Figure 10: Triangular efficiency across the year

The thermal efficiency and the exergy efficiency of the turbine using different fluids show a fairly constant behavior at different ambient temperature across the year. R245fa shows the lowest total-to-static efficiency, attributed to the supersonic expansion across the turbine. It is interesting to note that the turbine using R245fa shows the highest exergy efficiency though the thermal efficiency is the lowest among the three fluids. The high exergy efficiency using R245fa is attributed to the lowest entropy drop during the expansion across the turbine at different pressure ratio, as shown in Fig. 12.

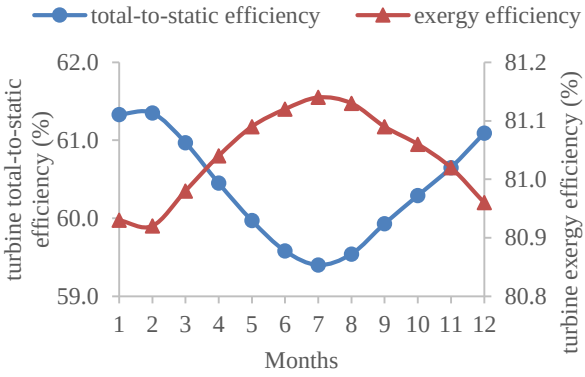

(a)

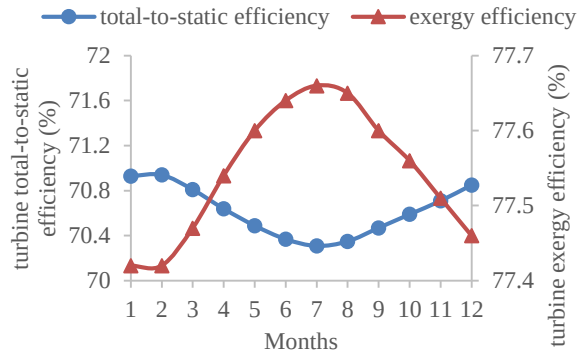

(b)

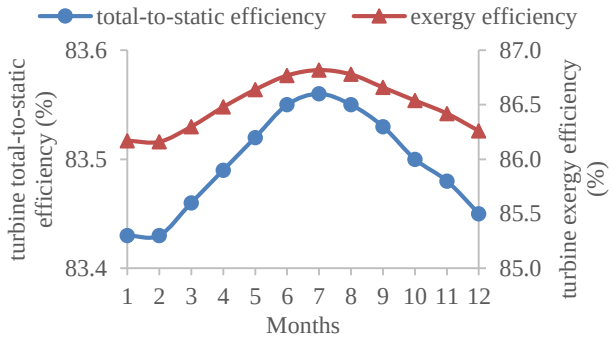

(c)

Figure 11: Thermal efficiency and exergy efficiency of the gas turbine using R245fa (a), isobutane (b), and R134a (c) across the year

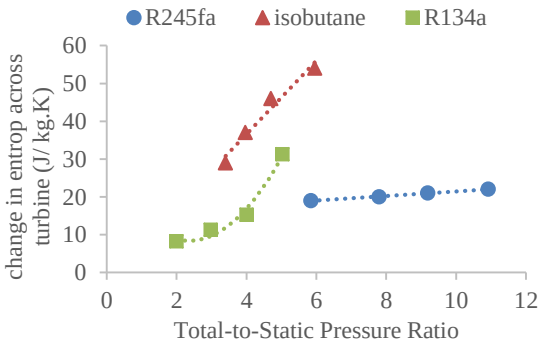

Figure 12: Change in entropy across the turbine at different pressure ratio

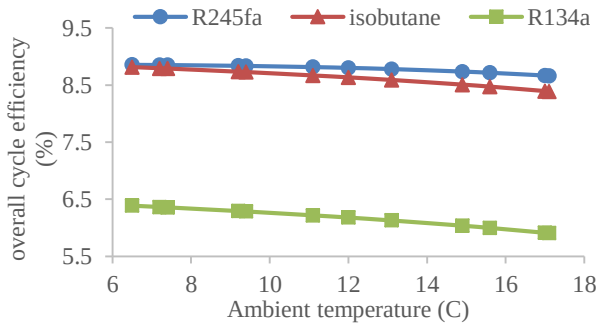

Figure 13: Thermal efficiency of the binary cycle as a function of ambient temperature

The thermal efficiency of the binary cycle decreases with the rise in ambient temperature. At higher ambient temperature, the differential temperature between the heat sink and the heat source is lower, hence reducing the cycle thermal efficiency. The thermal efficiency of the turbine, however, increases with the rise in ambient temperature. The ambient temperature increases and the pressure ratio across the turbine reduces over winter. Fig .7 and Fig. 12 show that the operation of the selected gas turbine is favorable at low pressure ratio over winter with higher total-to-static efficiency and lower entropy change. The exergy efficiency of the binary plant increases with respect to the ambient temperature, as the available

maximum theoretical work output from the cycle reduces with increase in ambient temperature, as shown in Fig. 15. The overall cycle efficiency is much lower than the triangular cycle efficiency from Fig. 10. The discrepancy in the cycle performance might be attributed to the following factors.

1. The low evaporating temperature within the vaporizer using R245fa, isobutane and R134a contributes to a large degree of differential temperature at the pinch of the vaporizer as shown in Fig. 14. The larger the pinch point differential temperature, the smaller the cycle thermal efficiency (Guo, Wang, & Zhang, 2011).
2. The heating curve of the working fluid within the vaporizer does not match with the heat source as phase change occurs within the vaporizer for a sub-critical ORC system, as shown in Fig. 14. The mismatch increases the irreversibility during the heat transfer across the vaporizer. A more thorough explanation of this phenomena can be found here (Stijepovic, Linke, Papadopoulos, & Grujic, 2012).

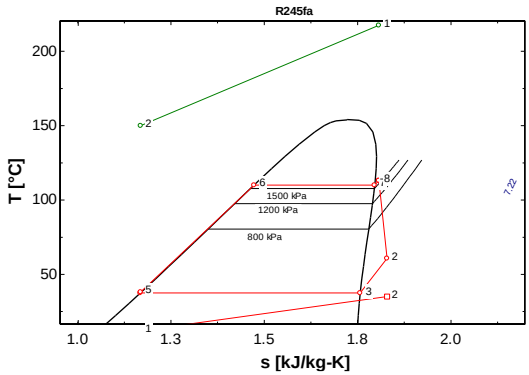

Figure 14: Simulation of binary plant using R245fa

The exergy efficiency and the thermal efficiency of the binary plant are dependent on the working fluids and the degree of superheat. Both isobutane and R245fa show a similar trend of the cycle thermal efficiency and exergy efficiency, with the same degree of superheat despite the difference in the maximum temperature of the working fluids within the cycle. R134a shows a similar trend of efficiency as a function of ambient temperature, with the curve shifted downwards at 2.5% and 3.5% for the thermal efficiency and the exergy efficiency, respectively.

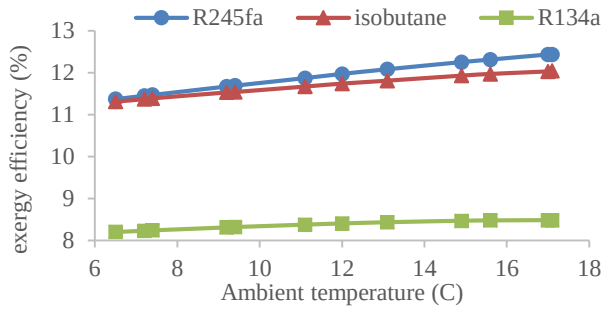

Figure 15: Exergy efficiency of the binary cycle as a function of ambient temperature

The following correlations were approximated from Fig. 13 and Fig.15 between the cycle thermal efficiency and exergy efficiency as a function of ambient temperature.

$$\eta_{I,cycle} = -0.04 T_{amb} + \eta_{I,cycle,0} \quad (11)$$

$\eta_{I,cycle,0}$ is the cycle thermal efficiency when the ambient temperature is 0°C, and T_{amb} is the air ambient temperature for any ACC binary plant, in degree Celsius.

$$\eta_{II,cycle} = -0.0018\left(T_{amb}\right)^2 + 0.1\left(T_{amb}\right) + \eta_{II,cycle,0} \quad (12)$$

$\eta_{II,cycle,0}$ is the cycle exergy efficiency when the ambient temperature is 0°C. Eq. (11) and (12) are only valid for subcritical ORC system since trans-critical ORC system is beyond the scope of this paper. A more thorough analysis is required to correlate the cycle performance to different inlet condition with different amount of superheat and sub-cooling.

4. CONCLUSION

Adaptation of an existing gas turbine as an ORC turbine is feasible as long as care is taken to adjust the operating conditions to the working fluid. In addition the generator must be modified to accommodate the new rotational speed of the turbine. The shaft speed can be determined at optimal velocity ratio, which is usually in the range of 0.6 and 0.7. The optimal rotational speed is different, depending on the working fluids. The adapted gas turbine was originally designed for sub-sonic expansion process. The turbine shows a higher thermal efficiency using R134a and isobutane in subsonic expansion process and a lower thermal efficiency using R245fa in supersonic expansion process. The exergy efficiency of the turbine is, however, higher in supersonic expansion due to the lower change in entropy at different pressure ratio.

The turbine shows a fairly constant thermal efficiency and exergy efficiency at different ambient temperature across the year. The binary cycle, however shows a small decrease in thermal efficiency and a slight increase in exergy efficiency when the ambient temperature increases. Both thermal and exergy efficiency are dependent on the type of working fluids, ambient temperature, degree of superheat, and type of operation (sub-critical cycle or trans-critical cycle). The thermal efficiency and the exergy efficiency of a simple binary cycle can be represented by model derived correlations, eq. (11) and (12) to investigate the overall performance of a binary cycle as a function of ambient temperature.

ACKNOWLEDGEMENTS

This work was supported by the Heavy Engineering Education Research foundation (HEERF) scholarship.

REFERENCES

Aneke, M., Agnew, B., & Underwood, C. (2011). Performance analysis of the Chena binary geothermal power plant. Applied Thermal Engineering, 31(10), 1825-1832. doi: http://dx.doi.org/10.1016/j.applthermaleng.2011.02.028

Astolfi, M., Romano, M. C., Bombarda, P., & Macchi, E. (2014). Binary ORC (organic Rankine cycles) power

plants for the exploitation of medium–low temperature geothermal sources – Part A: Thermodynamic optimization. Energy, 66(0), 423-434. doi: http://dx.doi.org/10.1016/j.energy.2013.11.056
Balje, O. E. (1981). Turbomachines: A Guide to Design Selection and Theory: Wiley.
Bertani, R. (2005). World geothermal power generation in the period 2001–2005. Geothermics, 34(6), 651-690.
Bertani, R. (2012). Geothermal power generation in the world 2005–2010 update report. Geothermics, 41(0), 1-29. doi: http://dx.doi.org/10.1016/j.geothermics.2011.10.001
Chen, H., Goswami, D. Y., & Stefanakos, E. K. (2010). A review of thermodynamic cycles and working fluids for the conversion of low-grade heat. Renewable and Sustainable Energy Reviews, 14(9), 3059-3067.
DiPippo, R. (2004). Second law assessment of binary plants generating power from low-temperature geothermal fluids. Geothermics, 33(5), 565-586.
DiPippo, R. (2012). Geothermal power plants: principles, applications, case studies and environmental impact: Butterworth-Heinemann.
Dunstall, M. (1999). Small Power Plants: Recent Developments in Geothermal Power Generation in New Zealand. Geo-Heat Center Quarterly Bulletin.
Ghasemi, H., Paci, M., Tizzanini, A., & Mitsos, A. (2013). Modeling and optimization of a binary geothermal power plant. Energy, 50(0), 412-428. doi: http://dx.doi.org/10.1016/j.energy.2012.10.039
Guo, T., Wang, H., & Zhang, S. (2011). Selection of working fluids for a novel low-temperature geothermally-powered ORC based cogeneration system. Energy Conversion and Management.
Holdmann, G. (2007). The Chena Hot Springs 400kW geothermal power plant: experience gained during the first year of operation. Chena Geothermal Power Plant Report, Chena Power Plant, Alaska, 1-9.
Jones, A. C. (1996). Design and Test of a Small, High Pressure Ratio Radial Turbine. Journal of Turbomachinery, 118(2), 362-370. doi: 10.1115/1.2836651
Kanoğlu, M., & Çengel, Y. A. (1999). Improving the Performance of an Existing Air-Cooled Binary Geothermal Power Plant: A Case Study. Journal of Energy Resources Technology, 121(3), 196-202. doi: 10.1115/1.2795982
Legmann, H., & Sullivan, P. (2003). The 30 MW Rotokawa I geothermal project five years of operation. Paper presented at the International Geothermal Conference.
Li, J., Pei, G., Li, Y., Wang, D., & Ji, J. (2012). Energetic and exergetic investigation of an organic Rankine cycle at different heat source temperatures. Energy, 38(1), 85-95. doi: http://dx.doi.org/10.1016/j.energy.2011.12.032
Lukawski, M. (2010). Design and optimization of standardized organic Rankine cycle power plant for European conditions.
Mendrinos, D., Kontoleontos, E., & Karytsas, C. (2012). Geothermal binary plants: Water or air cooled? Centre for Renewable Energy Sources. Greece. Accessed May, 30.
Mines, G. L. (2002). Evaluation of the impact of off-design operation on an air-cooled binary power plant. Transactions - Geothermal Resources Council, 701-706.
Moustapha, H., Zelesky, M., Baines, N. C., & Japiske, D. (2003). Axial and Radial Turbines: Concepts Eti.
NIWA. (2014). The National Climate Database.
Sauret, E. (2012). Open design of high pressure ratio radial-inflow turbine for academic validation. Paper presented at the Proceedings of the ASME 2012 International Mechanical Engineering Congress and Exposition, Houston, Texas.
Stijepovic, M. Z., Linke, P., Papadopoulos, A. I., & Grujic, A. S. (2012). On the role of working fluid properties in Organic Rankine Cycle performance. Applied Thermal Engineering, 36, 406-413. doi: 10.1016/j.applthermaleng.2011.10.057
Thain, I. A., & Carey, B. (2009). Fifty years of geothermal power generation at Wairakei. Geothermics, 38(1), 48-63. doi: http://dx.doi.org/10.1016/j.geothermics.2008.12.004
Wendt, D., & Mines, G. (2011). Effect of Ambient Design Temperature on Air-Cooled Binary Plant Output. Idaho: DoE Idaho National Laboratory.
Zarrouk, S. J., & Moon, H. (2014). Efficiency of geothermal power plants: A worldwide review. Geothermics, 51(0), 142-153. doi: http://dx.doi.org/10.1016/j.geothermics.2013.11.001